Dalton Transactions

ROYAL SOCIETY OF CHEMISTRY

PAPER

View Article Online
View Journal | View Issue

Check for updates

Cite this: *Dalton Trans.*, 2023, **52**, 3137

Synthesis of π-extended and bowl-shaped sumanene–ferrocene conjugates and their application in highly selective and sensitive cesium cations electrochemical sensors†

Jakub S. Cyniak,[a] Łucja Kocobolska,[a] Natalia Bojdecka,[a] Aleksandra Gajda-Walczak,[b] Agata Kowalczyk,[b] Barbara Wagner,[c] Anna M. Nowicka,[b] Hidehiro Sakurai[d,e] and Artur Kasprzak *[a]

Received 10th January 2023,
Accepted 13th February 2023

DOI: 10.1039/d3dt00084b

rsc.li/dalton

Carbon–carbon bond formation, condensation or *click chemistry* reactions were used to synthesize novel bowl-shaped sumanene–ferrocene conjugates, along with the extended π-electron framework in good yields. For the first time, the present study uses sumanene derivatives tris-substituted at the benzylic positions as the materials to begin the study on the *click chemistry* or the metal-catalyzed coupling reactions, Suzuki–Miyaura or Sonogashira couplings. The synthesized conjugates exhibited the property of selective recognizing cesium cations. As a result, this led to the development of highly sensitive and selective fluorescent or electrochemical sensors dedicated to the recognition of cesium cations (Cs^+) in water. We successfully designed the Cs^+ electrochemical sensors, which exhibited an acceptable limit of detection (LOD) values at 0.05–0.38 μM. Spectrofluorimetry, voltammetry, and laser ablation inductively coupled plasma mass spectrometry (LA-ICP-MS) were used to perform the selectivity studies. The results revealed that the designed sensors are highly Cs^+-selective. This work significantly contributes to the design of new methods of sumanene modification. It also provides further information on the electrochemical properties and innovative applications of metallocene-tethered sumanene derivatives.

Introduction

Sumanene (**1**) is a bowl-shaped compound, first synthesized in 2003,[1,2] and is a fragment of fullerene C_{60} (Fig. 1a). The compound belongs to the class of the so-called *buckybowls* and features several interesting physicochemical properties related to its specific bowl shape.[3–8] Due to the presence of both aromatic and benzylic moieties in the structure of sumanene, the synthetic view of the compound offers interesting opportunities for organic chemists. There have been several demonstrations over the years of the functionalization of sumanene at those positions, as represented by the successful attempts on the electrophilic aromatic substitution (S_EAr) reaction,[9–11] or reactions including sumanenyl benzylic anions.[12,13] As a result, there have been studies reporting several functional organic materials bearing the sumanene skeleton and featuring interesting properties and functions.[10,14–18]

Over the years, there have been theoretical[19–21] and experimental[22–26] studies on the interactions of sumanene with metal cations. The interaction of sumanene and its derivatives with cesium cations, which results in the formation of the sandwich-type complex is particularly fascinating (Fig. 1b). This interaction occurs in the anionic[25] or neutral[27–30] state of sumanene and occurs due to the perfect size match between the concave site of the sumanene bowl and the cesium cation's van der Waals radius. Recently, it was demonstrated that sumanene derivatives were used as fluorescent[27,29,30] or electrochemical[27,28] receptors of cesium cations. The interaction is remarkably specific and has no interfering effects from other cations, including rubidium cations.[31,32] The results of the studies have great environmental importance due to significant concentrations of radio-

[a]*Faculty of Chemistry, Warsaw University of Technology, Noakowskiego Str. 3, 00-664 Warsaw, Poland. E-mail: artur.kasprzak@pw.edu.pl*
[b]*Faculty of Chemistry, University of Warsaw, Pasteura Str. 1, 02-093 Warsaw, Poland*
[c]*Biological and Chemical Research Centre, Faculty of Chemistry, University of Warsaw, Zwirki i Wigury Str. 101, 02-093 Warsaw, Poland*
[d]*Division of Applied Chemistry, Graduate School of Engineering, Osaka University, 2-1 Yamadaoka, Suita, 565-0871 Osaka, Japan*
[e]*Innovative Catalysis Science Division, Institute for Open and Transdisciplinary Research Initiatives (ICS-OTRI), Osaka University, Suita, Osaka 565-0871, Japan*

†Electronic supplementary information (ESI) available: Experimental section, compounds characterization data, discussion on the NMR spectra, data on the spectrofluorimetric analyses of the complexes, calculation details. See DOI: https://doi.org/10.1039/d3dt00084b

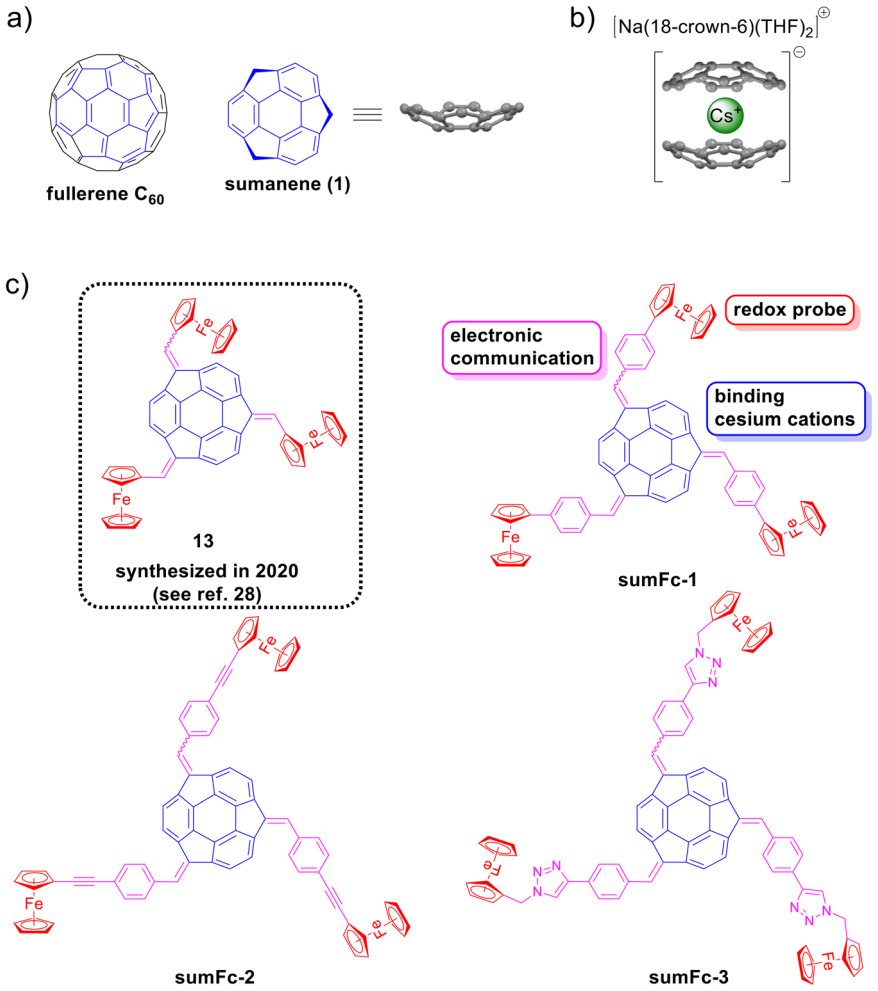

Fig. 1 (a) The structure of sumanene (**1**) and representation of its fullerene origin; (b) example of the sandwich complex composed of one cesium cation encapsulated by two sumanene bowls; (c) structures of compound **13** and the target **sumFc-1–sumFc-3** together with the graphical representation of the function of each building element.

active cesium isotopes, including Cs^{137}, were found in post-disaster areas of nuclear plant accidents in Fukushima and Chernobyl.[33–36]

In this study, the synthesis of novel sumanene–ferrocene conjugates **sumFc-1–sumFc-3** (Fig. 1c) and their application as receptor layers in electrochemical sensors to detect cesium cations in water is reported. The study focused on introducing copper-catalyzed azide–alkyne cycloaddition (CuAAC; *click chemistry*) or Sonogashira cross-coupling as new tools for sumanene derivatization. While the *click chemistry* reaction is eagerly used in the synthesis of functional organic compounds,[37–39] there are no reports on its use in the modification of sumanene. The design of *click chemistry* protocol for sumanene chemistry might offer new ways of modification of this bowl-shaped compound, due to the commercial availability or the easiness of preparation of various azide- or alkyne-containing molecules, as well as applicability of *click chemistry* reactions under aqueous conditions. Additionally, Sonogashira cross-coupling can likely be considered as a method for the expansion of π-electron system of sumanene. However, currently, 2-ethynylsumanene[3] is the only very preliminary[40] example of sumanene derivatized with Sonogashira cross-coupling.

Additionally, the study used sumanene derivatives tris-substituted at the benzylic positions for the first time as the starting materials in CuAAC or metal-catalyzed coupling reactions, namely Suzuki–Miyaura or Sonogashira couplings. The study further anticipated the enhanced electronic communication between the ferrocene units (redox probe) and sumanene (receptor site) in those compounds, considering the expansion of π-electron networks in **sumFc-1–sumFc-3** (see Fig. 1c). We suspected that this would result in good optical and beneficial properties of the electrochemical sensors. Thus, inspired by the our recent preliminary work[28] on tris(ferrocenylmethidene)sumanene (**13**) in electrochemical sensors, herein the successful design of highly selective and sensitive cesium cations electrochemical sensors comprising **sumFc-1–sumFc-3** in the role of receptor layers is reported.

Results and discussion

The synthesis of sumanene–ferrocene conjugates **sumFc-1–sumFc-3** is presented in Scheme 1. For the full experimental details, see section 1 in ESI.†

The synthesis of sumanene–ferrocene conjugate **sumFc-1** (Scheme 1a) was based on a two-step process. In the first stage, the Suzuki–Miyaura cross-coupling reaction was used to synthesize 4-(formylphenyl)ferrocene (**4**) in good yield (63%) from ferroceneboronic acid (**2**). In the second stage, the condensation-type reaction (isolated yield: 60%) was employed to synthesize the compound **sumFc-1** from sumanene (**1**) and compound **4**. The condensation occurred under phase transfer catalyst (PTC) conditions[13,28,29] with sodium hydroxide as a base and *n*-tetrabutylammonium bromide (TBAB) as a PTC catalyst.

Two synthetic pathways toward sumanene–ferrocene conjugate **sumFc-2** were studied (Scheme 1b). Both synthetic pathways consisted of two steps and were based on the Sonogashira cross-coupling and condensation-type reactions. There were differences in the reaction sequence in the synthetic pathways. In the first synthetic path, the ferrocene derivative bearing an aldehyde group was synthesized using the Sonogashira cross-coupling and was further subjected to the condensation-type reaction with sumanene (**1**). In the second path, the sumanene derivative bearing the halogen group was synthesized *via* the condensation-type reaction. Following this, it was subjected to the Sonogashira cross-coupling reaction with ethynylferrocene (**5**). In the first stage of the first synthetic path toward **sumFc-2**, a Sonogashira cross-coupling reaction was used to synthesize compound **7** from ethynylferrocene (**5**). In the second stage, compound **7** was subjected to the condensation-type reaction with sumanene (**1**). There were high yields for both steps (84–86%). In the second synthetic path toward **sumFc-2**, sumanene (**1**) was subjected to the condensation-type reaction with 4-iodobenzaldehyde (**6**), which yielded tris[(4-iodophenyl)methidene]sumanene (**8a**; 62%). Sonogashira cross-coupling reaction was used to synthesize the target **sumFc-2** from **8a** and **5**. The reaction yield was very high and equaled 95%. The reactivity of the respective tris[(4-bromophenyl)methidene]sumanene (**8b**) in the Sonogashira cross-coupling reaction with **5** was also investigated. The yield of **sumFc-2** synthesis starting from **8b** was significantly lower (52%) compared to the reaction yield starting from tris-iodo sumanene derivative **8a**. This denotes that the reactivity of halogen-containing bowl-shaped π-conjugated sumanene derivatives shall follow the general trend of the reactivity of aromatic halides in the Sonogashira cross-coupling reaction.

The preliminary trials toward the synthesis of **sumFc-3** were based on a similar pathway as those mentioned above. The pathways included the modification of the ferrocene derivative in the first stage and the subsequent condensation-type reaction with sumanene (Scheme 1c) in the second stage. The CuAAC reaction was employed to synthesize 1,2,3-triazole containing ferrocene derivative **11** efficiently (75%) from ferrocenemethylazide (**9**). Newly synthesized compound **11** was subjected to the condensation-type reaction with sumanene. However, despite several attempts, the target product **sumFc-3** was not obtained. We suspected that this resulted due to the presence of an active methylene group in **11**, which under basic conditions would likely interfere with the expected reaction pathway. In order to omit this severe limitation, the second synthetic pathway toward **sumFc-3** was studied. In the first stage, tris[(4-ethynylphenyl)methidene]sumanene (**12**) was synthesized from sumanene using the condensation-type reaction. This alkyne containing sumanene derivative was then used as the starting material in the synthesis of **sumFc-3**. The CuAAC reaction between **9** and **12** enabled the efficient (74%) synthesis of target **sumFc-3**. It is to be noted that **sumFc-3** is the first example of a sumanene derivative synthesized employing the *click chemistry* reaction.

Sumanene–ferrocene conjugates **sumFc-1–sumFc-3** were analyzed using an NMR spectroscopy and a high-resolution mass spectrometry (HRMS). The NMR spectra of **sumFc-1–sumFc-3** consisted of signals originating due to the presence of C_3 symmetrical and asymmetrical diastereomer.[13,28,29] The NMR spectra and a detailed discussion on the NMR spectra of **sumFc-1–sumFc-3** are presented in section 2 of the ESI.† Briefly, 7–9 signals or 24–30 signals were observed in the ^{1}H NMR analyses for symmetrical or unsymmetrical diastereomers, respectively. There were 16–19 signals or 48–57 signals in the $^{13}C\{^1H\}$ NMR analyses for symmetrical or unsymmetrical diastereomers, respectively. Due to the overlapped signals observed in the NMR spectra, the presence of many multiplets in the spectra was observed. In each case, the observed number of signals was highly consisted with the anticipated values, also within the given groups of multiplets originating from the presence of structural motifs introduced to the sumanene framework. The analysis of the cross-coupling signals in the ^{1}H–^{1}H COSY NMR spectra supported the proper assignments of the signals, as presented graphically in Fig. 2 for the representative sumanene derivative **sumFc-1**. Additionally, the signals originating from the presence of ferrocene in the synthesized compounds overlapped in the ^{1}H NMR and $^{13}C\{^1H\}$ NMR spectra. Therefore, the ^{1}H–^{13}C HSQC NMR analyses were especially helpful in supporting the ascription of the signals, which originated due to the presence of ferrocene in the synthesized conjugates **sumFc-1–sumFc-3** (see Fig. S45 in section 2 in ESI†).

To our delight, despite relatively sophisticated structures, compounds **sumFc-1–sumFc-3** exhibited good solubility in many commonly used organic solvents, including chloroalkanes (chloroform, dichloromethane, 1,2-dichloroethane), aromatics (benzene, toluene, chlorobenzene, *o*-dichlorobenzene), dimethylsulfoxide or tetrahydrofuran. The absorption spectra of **sumFc-1–sumFc-3** featured three absorption maxima (λ_{max}) located at 260–278 nm, 365–370 nm and 480–510 nm (for the spectra, see section 4 in ESI†). In comparison to the absorption spectrum of sumanene (**1**; λ_{max} = 278 cm^{-1} in CH_2Cl_2 [11,41]), the presence of two batochromically shifted absorption maxima for **sumFc-1–sumFc-3** was observed. It was

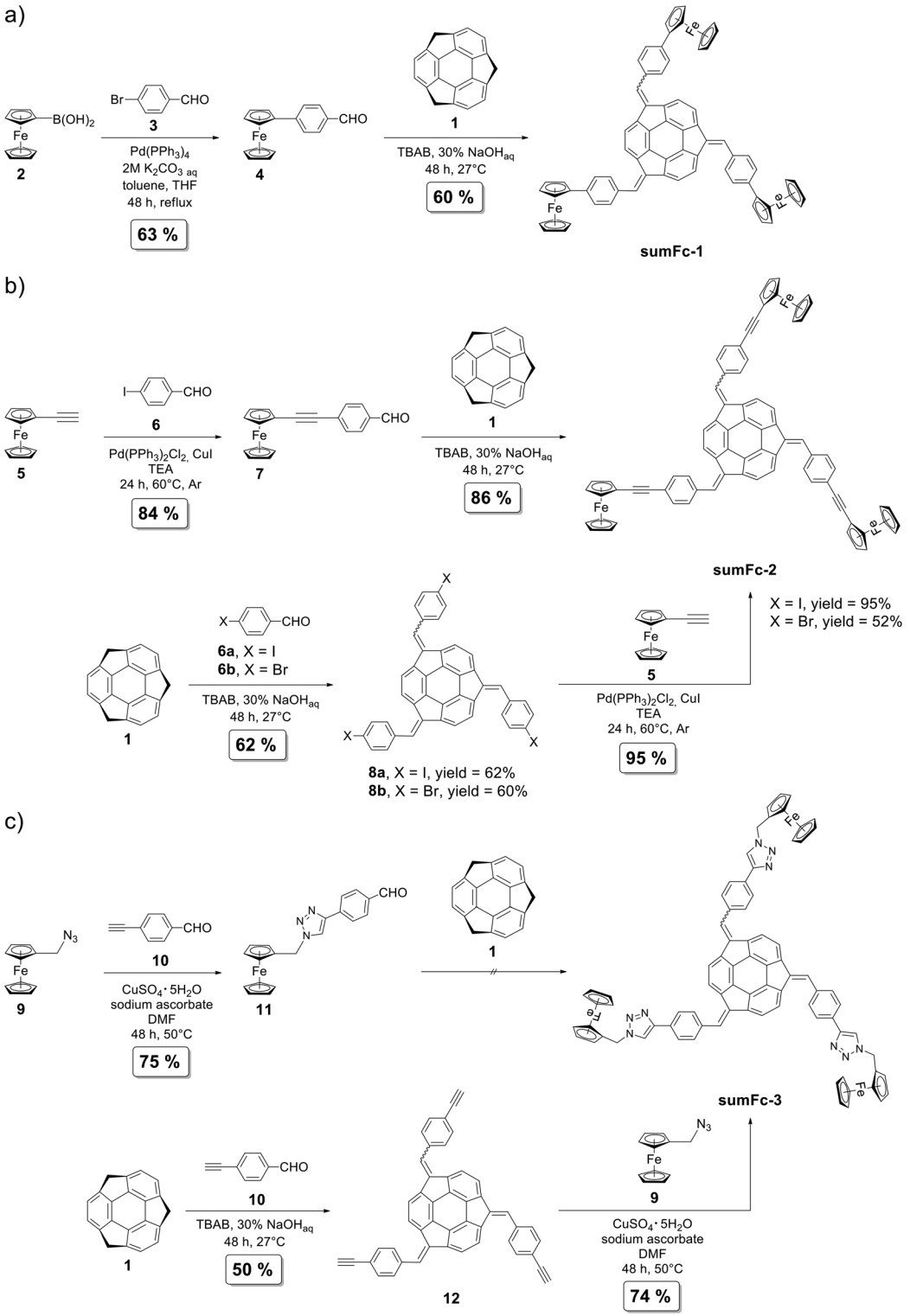

Scheme 1 Synthesis of sumanene–ferrocene conjugates **sumFc-1–sumFc-3**.

ascribed[13,28] to the expansion of π-electron system and the presence of ferrocene units in **sumFc-1–sumFc-3** structures. The highest emission intensity was found for compound **sumFc-3** (for the spectra, see section 4, ESI†).

As discussed above, the presence of sumanene skeleton in **sumFc-1–sumFc-3** opens up the possibility of the selective recognition of cesium cations by the compounds. At first, spectrofluorimetry was used to track the supramolecular inter-

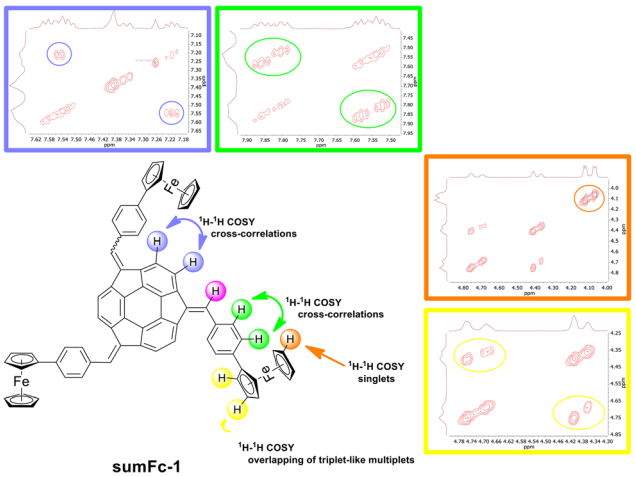

Fig. 2 The graphical representation of the cross-correlations in the ^{1}H–^{1}H COSY NMR spectra of sumanene–ferrocene conjugate **sumFc-1** together with the crucial insets of this spectra. The same color does not correspond to the same chemical shift in the NMR spectrum. For the detailed discussion on the NMR spectra of **sumFc-1–sumFc-3**, see section 2 in ESI.†

actions between the cesium cations and **sumFc-1–sumFc-3**. The addition of further portions (molar equivalents) of cesium cations caused a significant lowering of the emission intensity for each sumanene derivative. This is presented in Fig. 3a, for the representative compound **sumFc-3** (for the respective spectra for **sumFc-1** and **sumFc-2**, see section 5, ESI†). The dynamic interactions of the sumanene–ferrocene conjugates and cesium cations caused this turn-off behavior.[27,29,30] While there were further decreases in the emission intensity due to an increase in the cesium cations concentration, the changes were not the same at each interval. It was a direct result of the stoichiometry of the non-covalent systems formed. A continuous variation method (Job's plot method)[42] was employed to estimate stoichiometry for each system (see data in section 5, ESI†). A 2 : 1 stoichiometry (sumanene derivative : cesium cations) was concluded for each system. The stoichiometry corresponds to the anticipated sandwich-type complexes composed of one cesium cation encapsulated by two sumanene bowls.[27,29,30] Fig. 3b shows the illustrative visualization of the potential structure of those dynamically formed systems (for details of the calculation, refer to section 6 of ESI†).

The Benesi–Hildebrand method[29,30,43,44] was used to estimate the apparent binding constant (K_{app}) for each system. The values of K_{app} for newly synthesized sumanene–ferrocene conjugates **sumFc-1–sumFc-3** were comparable with the K_{app} values for other sumanene-based receptors.[27,29,30] The values were equaled to 3.3×10^4 M^{-2}, 8.4×10^4 M^{-2} and 7.3×10^4 M^{-2}, for **sumFc-1**, **sumFc-2**, and **sumFc-3**, respectively. The selectivity of the interaction between **sumFc-1–sumFc-3** and cesium cations was also investigated. There were no significant changes in the emission spectrum of **sumFc-1–sumFc-3** measured in the presence of 10 equivalents of rubidium cations. Since rubidium cations were previously reported to be

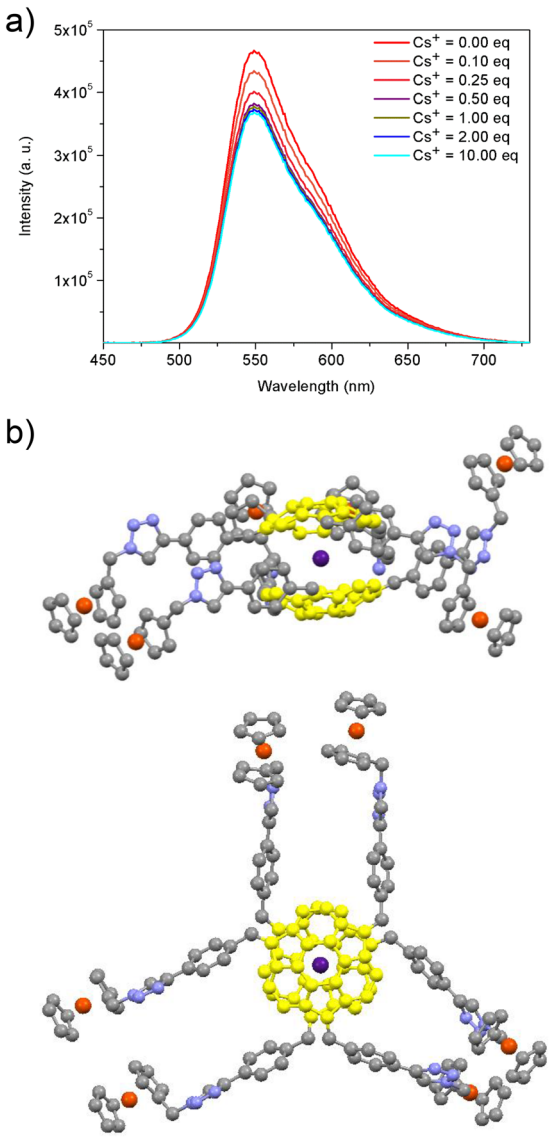

Fig. 3 (a) Emission spectra (λ_{ex} = 370 nm) of sumanene–ferrocene conjugate **sumFc-3** in the presence of various amounts (equivalents = eq) of cesium cations ($C_{sumFc-3}$ = 0.02 mM; solvent: $CHCl_3$: CH_3OH = 1 : 1 v/v), (b) possible structure of the formed sandwich complex between the representative **sumFc-3** (two symmetrical diastereoisomers) and Cs^+ (PM6 optimized structure is presented; for clarity, hydrogens are omitted and the sumanene bowls are marked yellow; the views from two different perspectives are presented).

the major interferent to recognizing the cesium cations, this study supported that there was a high specificity in the interaction between cesium cations and **sumFc-1–sumFc-3**. Additionally, there was no interfering effect of other metal cations, *i.e.*, sodium cations, potassium cations, magnesium cations, calcium cations, or barium cations. The high Cs^+ selectivity of the designed receptors was ascribed to the perfect size match between sumanene concave site and van der Waals radius of cesium cations (*ca.* 3.4 Å). This conclusion is highly consistent with the reported results of theoretical[19,21,25] and

experimental[25,27,30] studies. This perfect size match favors the cation–π interactions toward the dynamic formation of the complex, as visualized in Fig. 3b.

The ferrocenylated derivatives of the C_3-symmetric non-bowl-shaped 1,3,5-triphenylbenzene were synthesized to elucidate the importance of the presence of sumanene skeleton in the receptors **sumFc-1–sumFc-3** toward enabling Cs^+ recognition. The derivatives were compounds **14** and **16**, featuring structural similarity to **sumFc-2** and **sumFc-3**, respectively (see Fig. 4). The experimental details on their synthesis are presented in section 1 in ESI.† For compounds **14** and **16**, no changes in emission intensity were found when the spectra were measured even in the presence of the excess (10 eq.) of cesium cations (see Fig. 4 and data in section 6 in ESI†). Therefore, there was no interaction of **14** and **16** in a solution with cesium cations. This supports the crucial role of the presence of sumanene skeleton in compounds **sumFc-1–sumFc-3** to provide the Cs^+ recognition ability of those receptors.

The presence of ferrocene in the sumanene–ferrocene conjugates **sumFc-1–sumFc-3** makes them electroactive. The electrochemical characterization of **sumFc-1–sumFc-3** was performed in DCM with the addition of 100 mM $TBAPF_6$ as the supporting electrolyte. The representative cyclic voltammograms are presented in Fig. 5. One pair of the well-defined current signals, related to the Fc/Fc^+ electrode process was visible on the voltammetric curves. It shows that all Fc molecules are oxidized or reduced at the same potential. The intensity of the currents signals in the studied scan rate range (0.005 to 1.0 V s^{-1}) changed linearly with the square root of the scan rate. The insets in Fig. 5 present only the dependencies of $I_{ox,Fc}$ *versus* $v^{0.5}$. The linear character of the plotted dependencies $I_{ox,\ Fc} = f(v^{0.5})$ indicates the diffusive nature of each electrode process in each studied compound. The intensity of the current signal in the case of diffusion controlled reversible or quasi-reversible electrochemical process is described by the Randles–Sevcik equation[45] (eqn (1)):

$$I_{Fc} = 2.69 \times 10^5 n^{3/2} D^{1/2} A C_0 v^{0.5} \quad (1)$$

where: I_p is the peak current (anodic or cathodic), n – number of electron exchange during electrode process, A – the surface area of the working electrode, D – the diffusion coefficient of the electroactive species, C_0 – concentration of the electroactive species and v – the scan rate of voltammograms. The diffusion coefficients for the studied ferrocene–sumanene derivatives were determined from the slope of the plots $I_{ox,\ Fc} = f(v^{0.5})$. The obtained values of D as well as the regression equations are presented in Table 1. The values of the diffusion coefficients of the studied ferrocene–sumanene derivatives are very similar to each other and to the diffusion coefficient of native Fc (7.72×10^{-5} cm^2 s^{-1}).[46]

The receptor or analyte must have appropriate properties depending on the detection technique of the recognition

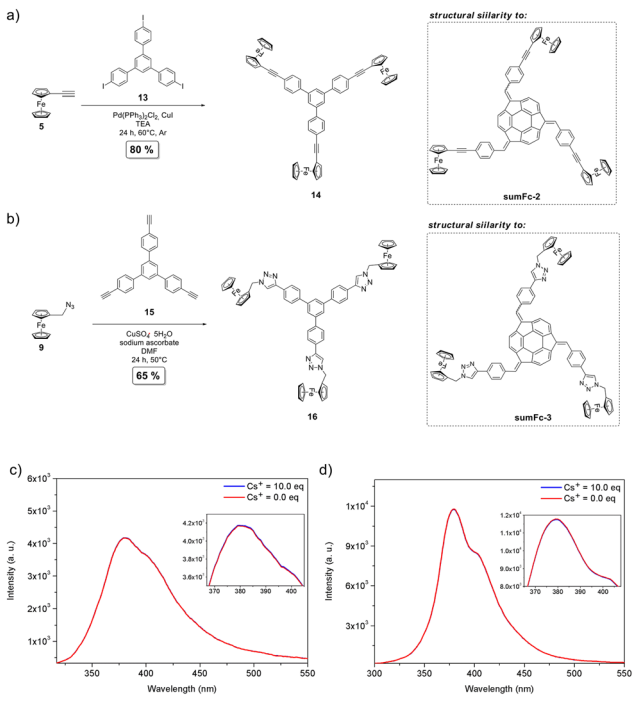

Fig. 4 (a and b) Synthesis of 1,3,5-triphenylbenzene-ferrocene conjugates **14** and **16**; (c and d) emission spectra (λ_{ex} = 290 nm) of compound **14** (c) and **16** (d) in the presence of 10 eq. (equivalents = eq) of cesium cations (C_{16} = 0.02 mM; solvent: $CHCl_3$: CH_3OH = 1 : 1 v/v; insets are also presented).

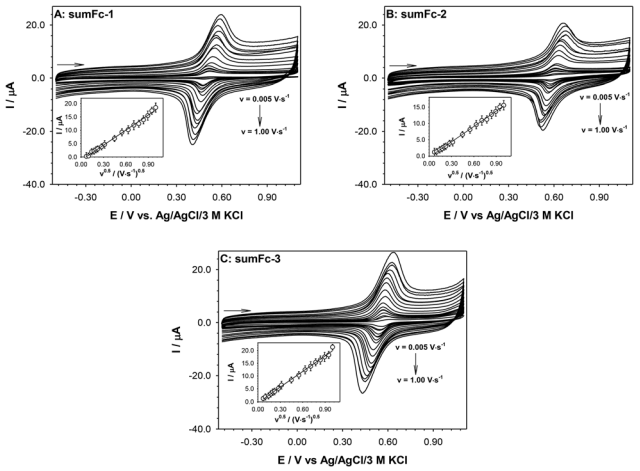

Fig. 5 Cyclic voltammograms of **sumFc-1** (A), **sumFc-2** (B) and **sumFc-3** (C) recorded in DCM. Experimental conditions: C_{sumFc} = 20 μM, C_{TBAPF_6} = 100 mM, T = 21 °C. Insets: dependencies of anodic peak currents *vs.* square root of scan rate.

Table 1 Values of the ferrocene–sumanene compounds diffusion coefficients and the regression equation of the dependencies $I_{ox,\ Fc} = f(v^{0.5})$

Compound	Regression equation	r	$D \times 10^5$ [cm^2 s^{-1}]
sumFc-1	$I_{Fc} = 18.77 \cdot v^{0.5} - 1.21$	0.9973	9.04
sumFc-2	$I_{Fc} = 15.72 \cdot v^{0.5} - 0.35$	0.9988	6.34
sumFc-3	$I_{Fc} = 20.20 \cdot v^{0.5} - 0.36$	0.9977	10.50

process, enabling the use of a specific measurement technique. The required condition for the electrochemical detection methods is electroactivity, *i.e.*, the ability of a molecule to replace an electron with the electrode surface. The electrochemical molecular recognition process should result in a change in the intensity of the current signal or a large shift in the redox potential of the analyte if it is electroactive, or an electroactive signaling unit. The signaling unit is usually performed by metallocenes, which include ferrocene and its derivatives. Thus, the first step was the voltammetric characterization of the containing receptor layers that contained the ferrocene-sumanene derivatives **sum-Fc-1–sum-Fc-3**. The cyclic voltammetry experiment was used to perform the electrochemical characteristics of the obtained receptor layers (GC/sumFc-TBAPF$_6$-nafion™). The measurements were carried out in 50 mM TBABF$_4$ aqueous solution. The recorded cyclic voltammograms for the various scan rates are presented in Fig. 6. The cyclic voltammograms of the recognition layers, obtained at the scan rates between 0.005 and 0.400 V s^{-1}, exhibited well-developed anodic peak. However, the cathodic peak was only visible in the case of **sumFc-1** and **sumFc-2**.

The electrode process should be a surface process since the studied sumanene–ferrocene receptors were immobilized on the electrode surface. In order to confirm this thesis, the dependencies of the anodic current signal intensity as a function of the electrode scan rate were plotted. The obtained dependencies are presented in the insets of Fig. 6. The linear dependencies of $I_{ox,\ Fc} = f(v)$ in the whole range of the studied scan rates were observed only for **sumFc-3**. The plotted dependencies of the **sumFc-1** and **sumFc-2** were linear in the range 0.005–0.075 V s^{-1}. It should be noted that the intensities of the anodic current signal concerning the square root of the scan rate for all studied ferrocene–sumanene derivatives also showed linearity. The receptors differ between each other in the structure and the length of the linker between sumanene molecule and the ferrocene units. The linear nature of the $I_{ox,\ Fc} = f(v^{0.5})$ relationship confirms the lability of the redox probe in the layer.

The ability to use **sumFc-1–sumFc-3** containing receptor layer in the detection of cesium cations (Cs^+) was instigated in the final stage of the research program. We decided to analyze the sensitivity of such a sensor, and whether it is influenced by the linker through which the ferrocene units are conjugated to the sumanene molecule. The sensitivity of the receptors to the presence of the Cs^+ in the solution was determined based on the changes in the ferrocene electrooxidation current signal intensity. Differential pulse (DP) voltammetry was used to carry out the measurements in water in the Cs^+ concentration ranging from 0.5 to 100 μM. The recorded DP voltammograms are presented in Fig. 7. The obtained DP voltammograms showed that with the increase in the Cs^+ concentration in the analyzed solution, there was also an increase in the intensity of the ferrocene electrooxidation current signal. The difference in the ferrocene current signal intensities, recorded in the presence and absence of the cesium cation, was used in the construction of the calibration curves ($I_{\mathrm{sumFc\cdots Cs^+}} - I_{\mathrm{sumFc}}$)·100% = $f(C_{Cs^+})$ (see insets in Fig. 7). The analytical parameters of the receptor layer were determined based on these curves, such as the linear regression equation, analytical range of work, limits of detection (LOD) and limits of quantification (LOQ). The values of these parameters are given in Table 2. The LOD and (LOQ) were determined for each receptor according to the equations:[45]

$$\mathrm{LOD} = \frac{3\sigma}{a} \tag{2}$$

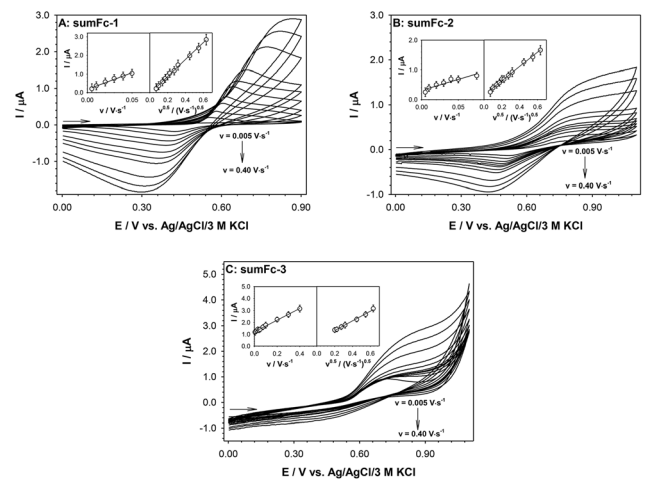

Fig. 6 Cyclic voltammograms of recognition layers (GC/sumFc-TBAPF$_6$-nafion™) containing: **sumFc-1** (A), **sumFc-2** (B) and **sumFc-3** (C) recorded in 50 mM TBABF$_4$ aqueous solution. Experimental conditions: C_{sumFc} = 20 μM, T = 21 °C. Insets: dependencies of anodic peak currents *vs.* scan rate and square root of scan rate.

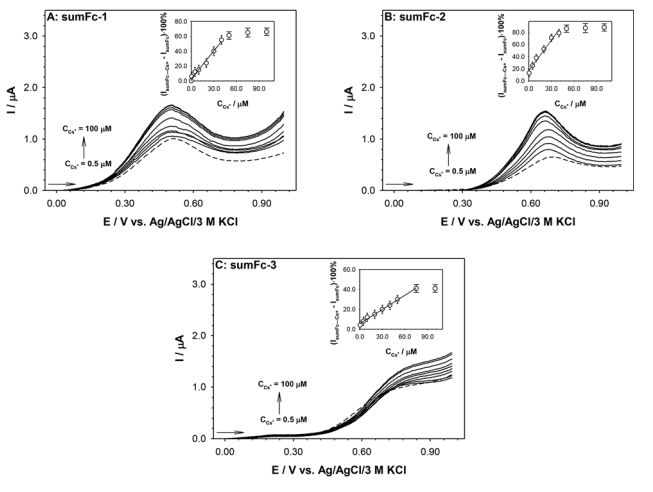

Fig. 7 DP voltammograms of recognition layers (GC/sumFc-TBAPF$_6$-nafion™) containing: **sumFc-1** (A), **sumFc-2** (B) and **sumFc-3** (C) recorded in 50 mM TBABF$_4$ aqueous solution with different addition of cesium cation. Experimental conditions: C_{sumFc} = 20 μM, T = 21 °C, modulation time: 0.002 s, interval time: 0.1 s, modulation amplitude: 0.04995 V. Insets: dependencies of anodic peak currents *vs.* Cs^+ concentration.

$$\mathrm{LOQ} = 3.3 \cdot \mathrm{LOD} \quad (3)$$

where: σ is the standard deviation of the response observed for the lowest measurable Cs^+ concentration and a is the slope of the calibration curve.

The lowest value of the limit of detection (LOD) had the sensor containing the **sumFc-1** receptor, what might be a result of the lowest K_{app} value (3.3×10^4 M^{-2} by spectrofluorimetry) for **sumFc-1** receptor. Notably, the sensors containing **sumFc-1** and **sumFc-2** that were synthesized by means of the carbon–carbon bond formation reaction (Suzuki–Miyaura and Sonogashira coupling, respectively) featured relatively similar LOD values (0.05–0.09 μM). The LOD value for the sensor containing **sumFc-3** was higher (0.38 μM). This difference might be a result of better electronic communication between sumanene and ferrocene units in **sumFc-1** and **sumFc-2** in comparison to the *click chemistry* derived **sumFc-3**.

The stability and selectivity of the receptors were also investigated. The electrochemical measurements were performed every 3 days. The sensors between the measurements were kept in the desiccator. There were no significant changes in the intensity and the position of the recorded current signal during the 2-month period. The observed differences were not higher than 4.5%. Based on the results described for the changes in the intensity of the Fc electrooxidation current signal since the construction of the sensor, it is concluded that the constructed sensor was very stable.

The selectivity studies were carried out against other cations: Na^+, K^+ and Ba^{2+}. The diagram is presented in Fig. 8. The influence of other metal cations on the Fc current signal was negligible. Thus, the electrochemical studies further indicated that the designed sensors are highly selective *versus* Cs^+. The laser ablation inductively coupled plasma mass spectrometry (LA-IC-MS) analysis was performed to further prove that the designed ferrocene–sumanene derivatives **sumFc-1–sumFc-3** are very selective receptors toward Cs^+. The substrate (glass), modified with the sumanene–ferrocene receptor, was immersed in an equimolar mixture of (20 μM) with Cs^+, Na^+, K^+, and Ba^{2+} for 1 hour before the measurements. Raw signals were background corrected for each isotope individually for Ar flow only. Spikes (defined as a single data point exceeding the intensities of the neighboring data more than 2 times) were replaced with a value of the average intensity of two neighboring signals. A custom-written formula in Excel® (Microsoft Corp.) was used for all the recalculations and visualization of the LA-ICP-MS data. Fluctuations of transient signals recorded during line ablation for the respective isotopes of Na, K, Fe, Cs, and Ba allowed for the calculation of correlation coefficients of co-occurrences of all elements against each other. A percentile scale, setting the maximum (red color) for the 95th percentile value and the minimum (white color) for the 5th percentile value, was used as a reference for the relative formatting of cells containing calculated correlation coefficients. The results obtained for three independent samples are presented in Fig. 9. The correlation coefficient indicating the co-occurrence of Fe with other elements for each sample was calculated in descending order: Cs > Na > Mg. However, there was no rule of constant behavior for K and Ba.

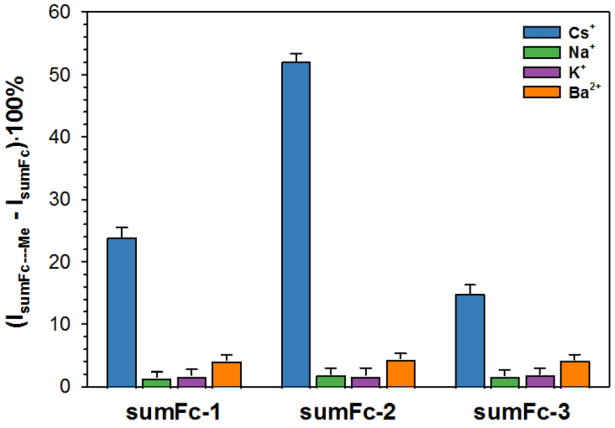

Fig. 8 Differences in the Fc current signal intensities recorded in the presence and absence of the interferent cations recorded for: **sumFc-1**, **sumFc-2** and **sumFc-3** in 50 mM $TBABF_4$ aqueous solution. Experimental conditions: C_{sumFc} = 20 μM, C_{Me^+} = 20 μM, T = 21 °C, modulation time: 0.002 s, interval time: 0.1 s, modulation amplitude: 0.04995 V.

The comparison of the LOD values for the designed electrochemical sensors, comprising **sumFc-1–sumFc-3** as the receptor layer, with the performance of the other reported Cs^+ receptors is presented in Table 3. As it can be seen, the LOD values for **sumFc-1–sumFc-3** are lower in comparison to the other, non-sumanene receptors. The better performance of sumanene-based receptors in comparison with the calixarene-based ones, is especially important, also from the viewpoint of the high Cs^+ selectivity of **sumFc-1–sumFc-3**. Notably, the performance of **sumFc-1–sumFc-3** and tris(ferrocenylmethidene)sumanene (**13**) based sensors is better than the performance of the monoferrocenylsumanenes. **SumFc-1** and **sumFc-2** together with tris(ferrocenylmethidene)sumanene (**13**), show the most satisfactory LOD values (0.02–0.09 μM). From the application viewpoint, it is also important that the sensors comprising **sumFc-1–sumFc-3** as the receptor layer featured good time stability.

Table 2 Values of the analytical parameters for Cs^+ detection using sensors containing receptor layers composed of **sumFc-1–sumFc-3**

Compound	Regression equation	r	Analytical work of range [μM]	LOD/LOQ [μM]
sumFc-1	$(I_{sumFc\cdots Cs+} - I_{sumFc})\cdot 100\% = 1.25\cdot C_{Cs^+} + 2.79$	0.9907	0.5–40	0.05/0.16
sumFc-2	$(I_{sumFc\cdots Cs+} - I_{sumFc})\cdot 100\% = 1.67\cdot C_{Cs^+} + 17.0$	0.9876	0.5–40	0.09/0.30
sumFc-3	$(I_{sumFc\cdots Cs+} - I_{sumFc})\cdot 100\% = 0.48\cdot C_{Cs^+} + 5.45$	0.9967	0.5–75	0.38/1.24

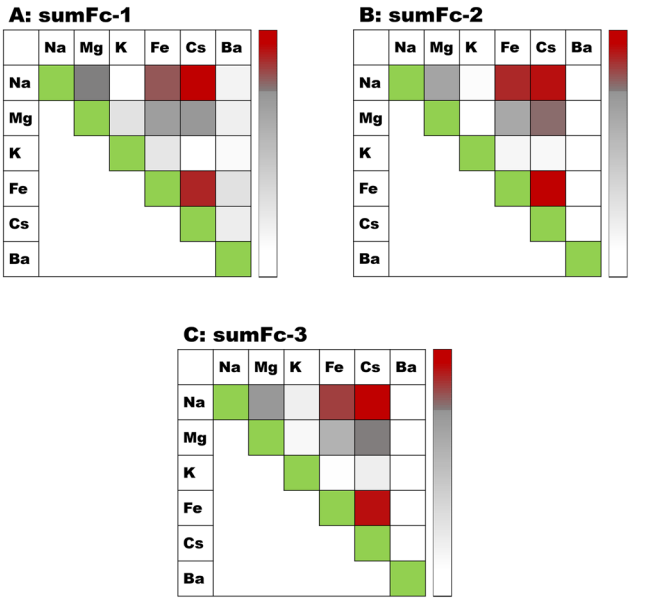

Fig. 9 The correlation coefficient values calculated from LA-ICP-MS results showing co-occurrence of Na, Mg, K, Fe, Cs and Ba over the samples **sumFc-1**, **sum-Fc2** and **sumFc-3**. The green squares indicate the value equal to 1.00 which were withdrawn from the comparison of elemental co-occurrence.

Table 3 Comparison of the LOD values for various Cs^+ receptors

Receptor	LOD [μM]	Ref.
sumFc-1	0.05	This work
sumFc-2	0.09	This work
sumFc-3	0.39	This work
Tris(ferrocenylmethidene)sumanene (**13**)	0.02	28
Monoferrocenylsumanenes	12–70	27
Zeolite KY	7.3	47
Squaraine	0.096	48
Calixarenes	0.096–0.770	49,50
Boron-dipyrromethene (BODIBY)	0.273	51

Conclusions

In conclusion, this work designed new, efficient methods of sumanene modification employing *click chemistry* of metal-catalyzed carbon–carbon bond formation reactions. As a result, novel, bowl-shaped, and π-extended sumanene derivatives bearing three ferrocene units (**sumFc-1**–**sumFc-3**) were synthesized. Sophisticated sumanene derivatives tris-substituted at the benzylic positions were used for the first time as the starting materials in the *click chemistry* reaction and Suzuki–Miyaura or Sonogashira couplings. Our findings significantly contribute to further development in sumanene chemistry toward the design of novel functional organic compounds bearing a sumanene motif. All the synthesized compounds have been comprehensively characterized with the spectroscopic techniques. Spectrofluorimetric analyzes revealed that compounds **sumFc-1**–**sumFc-3** selectively interact with cesium cations. The apparent binding constants for the dynamically formed sandwich-type complexes equals (3.3–7.3) × 10^4 M^{-2}. Voltammetry was used to electrochemically analyze the designed sumanene–ferrocene conjugates. Each compound featured one pair of well-defined current signals, which is related to the Fc/Fc^+ electrode process. Eventually, herein, the design of the electrochemical sensors toward the fast, sensitive, and selective detection of cesium cations (Cs^+) in water was described. The lowest limit of detection (LOD) of Cs^+ was found for **sumFc-1** containing sensor (0.05 μM). The LOD values for **sumFc-2** and **sumFc-3** containing sensors equaled 0.09 μM and 0.38 μM, respectively. The effect of the linker between the sumanene and ferrocene units in the studied conjugates on the LOD of Cs^+ sensors was observed. The sensors, which contained the carbon–carbon bonded **sumFc-1** (synthesized *via* Suzuki–Miyaura coupling) and **sumFc-2** (synthesized *via* Sonogashira coupling), featured lower LOD values (0.05–0.09 μM) compared to the *click chemistry* derived **sumFc-3** (0.38 μM). It might be ascribed to the better electronic communication between the sumanene and the ferrocene units in **sumFc-1** and **sumFc-2** compared to **sumFc-3**. Notably, these LOD values indicate the potential usefulness of the designed sensors in the analyses of real samples, such as the ones from post-disaster areas. For example, the Mano River (Japan, northwest of the Fukushima–Daiichi plant) contaminated with radioactive toxic cesium was estimated to be *ca.* 0.06 mM.[28,33] Eventually, the high selectivity of the designed sumanene–ferrocene receptors toward recognizing Cs^+ was also evidenced with fluorescence spectroscopy, electrochemistry, and laser ablation inductively coupled plasma mass spectrometry (LA-ICP-MS). Considering the presented results, this work significantly contributes to further the progress in the organic chemistry of sumanene by providing new protocols for its modification. Additionally, it broadens the knowledge of the electrochemical properties of the sumanene–ferrocene conjugates as well as their applications in environmental chemistry, especially Cs^+ detection.

Conflicts of interest

There are no conflicts to declare.

Acknowledgements

The financial support the National Science Centre, Poland, OPUS grant no. 2021/43/B/ST4/00114 (A. K.), Warsaw University of Technology (WUT; A. K.), and JSPS KAKENHI grant no. JP19H00912 and JP21H05233 (H. S.) are acknowledged. We would like to thank Dr hab. Mariola Koszytkowska-Stawińska, prof. WUT, for fruitful discussions, Mr Sergei Molchanov (WUT) for his assistance in 2-D NMR spectra measurements, and Mr Maurycy Krzyżanowski (WUT) for his assistance in calculation part.

References

1 H. Sakurai, T. Daiko and T. Hirao, *Science*, 2003, **301**, 1878–1878.
2 H. Sakurai, *Bull. Chem. Soc. Jpn.*, 2021, **94**, 1579–1587.
3 T. Amaya and T. Hirao, *Chem. Rec.*, 2015, **15**, 310–321.
4 T. Amaya and T. Hirao, *Chem. Commun.*, 2011, **47**, 10524.
5 S. Higashibayashi and H. Sakurai, *Chem. Lett.*, 2011, **40**, 122–128.
6 M. Saito, H. Shinokubo and H. Sakurai, *Mater. Chem. Front.*, 2018, **2**, 635–661.
7 S. Mebs, M. Weber, P. Luger, B. M. Schmidt, H. Sakurai, S. Higashibayashi, S. Onogi and D. Lentz, *Org. Biomol. Chem.*, 2012, **10**, 2218.
8 T.-C. Wu, H.-J. Hsin, M.-Y. Kuo, C.-H. Li and Y.-T. Wu, *J. Am. Chem. Soc.*, 2011, **133**, 16319–16321.
9 B. B. Shrestha, S. Karanjit, G. Panda, S. Higashibayashi and H. Sakurai, *Chem. Lett.*, 2013, **42**, 386–388.
10 I. Hisaki, H. Toda, H. Sato, N. Tohnai and H. Sakurai, *Angew. Chem., Int. Ed.*, 2017, **56**, 15294–15298.
11 H. Toda, Y. Uetake, Y. Yakiyama, H. Nakazawa, T. Kajitani, T. Fukushima and H. Sakurai, *Synthesis*, 2019, 4576–4581.
12 H. Sakurai, T. Daiko, H. Sakane, T. Amaya and T. Hirao, *J. Am. Chem. Soc.*, 2005, **127**, 11580–11581.
13 T. Amaya, K. Mori, H.-L. Wu, S. Ishida, J. Nakamura, K. Murata and T. Hirao, *Chem. Commun.*, 2007, 1902–1904.
14 T. Amaya, T. Nakata and T. Hirao, *J. Am. Chem. Soc.*, 2009, **131**, 10810–10811.
15 S. Alvi and R. Ali, *Beilstein J. Org. Chem.*, 2020, **16**, 2212–2259.
16 Y. Yakiyama, T. Hasegawa and H. Sakurai, *J. Am. Chem. Soc.*, 2019, **141**, 18099–18103.
17 Y. Shoji, T. Kajitani, F. Ishiwari, Q. Ding, H. Sato, H. Anetai, T. Akutagawa, H. Sakurai and T. Fukushima, *Chem. Sci.*, 2017, **8**, 8405–8410.
18 T. Amaya, K. Kobayashi and T. Hirao, *Asian J. Org. Chem.*, 2013, **2**, 642–645.
19 U. D. Priyakumar and G. N. Sastry, *Tetrahedron Lett.*, 2003, **44**, 6043–6046.
20 I. K. Petrushenko, N. V. Shipitsin and K. B. Petrushenko, *Phys. E*, 2022, **135**, 114949.
21 D. Vijay, H. Sakurai, V. Subramanian and G. N. Sastry, *Phys. Chem. Chem. Phys.*, 2012, **14**, 3057.
22 T. Amaya, W. Wang, H. Sakane, T. Moriuchi and T. Hirao, *Angew. Chem., Int. Ed.*, 2010, **49**, 403–406.
23 T. Amaya, H. Sakane and T. Hirao, *Angew. Chem.*, 2007, **119**, 8528–8531.
24 T. Amaya and T. Hirao, in *Advances in Organometallic Chemistry and Catalysis*, ed. A. J. L. Pombeiro, John Wiley & Sons, Inc., Hoboken, NJ, USA, 2013, pp. 473–483.
25 S. N. Spisak, Z. Wei, A. Yu. Rogachev, T. Amaya, T. Hirao and M. A. Petrukhina, *Angew. Chem., Int. Ed.*, 2017, **56**, 2582–2587.
26 T. Amaya, Y. Takahashi, T. Moriuchi and T. Hirao, *J. Am. Chem. Soc.*, 2014, **136**, 12794–12798.
27 A. Kasprzak and H. Sakurai, *Dalton Trans.*, 2019, **48**, 17147–17152.
28 A. Kasprzak, A. Kowalczyk, A. Jagielska, B. Wagner, A. M. Nowicka and H. Sakurai, *Dalton Trans.*, 2020, **49**, 9965–9971.
29 A. Kasprzak and H. Sakurai, *Chem. Commun.*, 2021, **57**, 343–346.
30 A. Kasprzak, A. Tobolska, H. Sakurai and W. Wróblewski, *Dalton Trans.*, 2022, **51**, 468–472.
31 D. Wu, A. C. Sedgwick, T. Gunnlaugsson, E. U. Akkaya, J. Yoon and T. D. James, *Chem. Soc. Rev.*, 2017, **46**, 7105–7123.
32 N. Kumar, I. Leray and A. Depauw, *Coord. Chem. Rev.*, 2016, **310**, 1–15.
33 T. Mizuno and H. Kubo, *Sci. Rep.*, 2013, **3**, 1742.
34 Y. Morino, T. Ohara and M. Nishizawa, *Geophys. Res. Lett.*, 2011, **38**, L00G11.
35 A. T. Kotilainen, M. M. Kotilainen, V.-P. Vartti, K.-L. Hutri and J. J. Virtasalo, *Mar. Pollut. Bull.*, 2021, **172**, 112924.
36 V. Saenko, V. Ivanov, A. Tsyb, T. Bogdanova, M. Tronko, Yu. Demidchik and S. Yamashita, *Clin. Oncol.*, 2011, **23**, 234–243.
37 P. Thirumurugan, D. Matosiuk and K. Jozwiak, *Chem. Rev.*, 2013, **113**, 4905–4979.
38 K. Sada and K. Kokado, in *Advances in Organic Crystal Chemistry*, ed. M. Sakamoto and H. Uekusa, Springer Singapore, Singapore, 2020, pp. 523–538.
39 Y. Goto, H. Sato, S. Shinkai and K. Sada, *J. Am. Chem. Soc.*, 2008, **130**, 14354–14355.
40 2-Ethynylsumanene was a part of unpublished results. This compound was introduced in the account (see ref. 3). No spectral data was provided for this compound. A preliminary trial on using this compound for the Glaser coupling reaction was reported (yield 12%; MALDI-MS data was provided for the Glaser coupling product, no NMR data was provided).
41 Q. Tan, P. Kaewmati, S. Higashibayashi, M. Kawano, Y. Yakiyama and H. Sakurai, *Bull. Chem. Soc. Jpn.*, 2018, **91**, 531–537.
42 J. S. Renny, L. L. Tomasevich, E. H. Tallmadge and D. B. Collum, *Angew. Chem., Int. Ed.*, 2013, **52**, 11998–12013.
43 H. A. Benesi and J. H. Hildebrand, *J. Am. Chem. Soc.*, 1949, **71**, 2703–2707.
44 S. Goswami, K. Aich, S. Das, A. K. Das, A. Manna and S. Halder, *Analyst*, 2013, **138**, 1903.
45 A. J. Bard and L. R. Faulkner, *Electrochemical methods: fundamentals and applications*, Wiley, New York, 2nd edn, 2001.
46 N. S. Neghmouche and T. Lanez, *Int. Lett. Chem., Phys. Astron.*, 2013, **9**, 37–45.
47 M. Arvand, M. Moghimi and M. A. Bagherinia, *Anal. Lett.*, 2009, **42**, 393–408.
48 B. Radaram, T. Mako and M. Levine, *Dalton Trans.*, 2013, **42**, 16276.

49 X. Q. Pham, L. Jonusauskaite, A. Depauw, N. Kumar, J. P. Lefevre, A. Perrier, M.-H. Ha-Thi and I. Leray, *J. Photochem. Photobiol., A*, 2018, **364**, 355–362.
50 N. Kumar, Q. Pham-Xuan, A. Depauw, M. Hemadi, N.-T. Ha-Duong, J.-P. Lefevre, M.-H. Ha-Thi and I. Leray, *New J. Chem.*, 2017, **41**, 7162–7170.
51 E. Özcan and B. Çoşut, *ChemistrySelect*, 2018, **3**, 7940–7944.